High operating temperature n-on-p extrinsic MWIR HgCdTe photodiodes

Maxence Soria, Pierre Bleuet, François Boulard, Jean-Louis Santailler, Florian Marmonier, Léo Bonnefond, Thierry Pellerin, Guillaume Poisson, Johan Rothman

High operating temperature n-on-p extrinsic MWIR HgCdTe photodiodes

M. Soria, P. Bleuet, F. Boulard, J.-L. Santailler, F. Marmonier, L. Bonnefond, T. Pellerin, G. Poisson and J. Rothman
Univ. Grenoble Alpes, CEA, Leti, F-38000 Grenoble, France

ABSTRACT

N-on-p extrinsically doped MWIR HgCdTe material and photodiodes have been developed to benefit from the expected reduction of the Auger generation in the p-type absorbing layer. Samples with two doping levels have been characterized using dark current, current noise, Hall effect and PhotoLuminescence Decay (PLD) measurements. The dark current and PLD measurements are consistent with a reduction of the Auger generation quantified by the ratio between the Auger 1 and 7 recombination coefficients γ around 10. The corresponding dark current in the sample with the lowest doping level was slightly higher than in typically p-on-n photodiodes. The low frequency noise, characterized by a Tobin coefficient below 10^{-5}, is lower than the values reported for other MWIR HgCdTe photodiodes at the same dark current density. The low dark current and dark current noise show on the high potential of such photodiodes to form focal plane array that can be operated at high operating temperature without degradation of the image quality.

Keywords: HgCdTe, p-type extrinsic doping, dark current, dark current noise, photoluminescence decay, minority carrier lifetime, midwave infrared, HOT

1. INTRODUCTION

One of the main challenges in the quantum infrared detection field is the increase of the operating temperature. Such improvement could allow to reduce the Size, Weight and Power-Cost (SWAPc) associated with the cooling system. This technological goal do not only require a low dark current but also an absence of low frequency fluctuations on the dark current that causes a deterioration of the image quality. Such detector is often termed High Operating Temperature (HOT) detector.

Dark current density and dark current noise are two key figures of merit to characterize a focal plane array development in terms of operating temperature. At a given operating temperature, the diffusion dark current density is inversely proportional to the product of the minority carrier lifetime times the majority carrier concentration in the absorption layer [1]. Thus, this product has to be optimized to reduce the diffusion dark current.

The ultimate achievable performance is limited by the Auger contribution to minority carrier lifetime in the absorption layer [2]. Hence, in $Hg_{1-x}Cd_xTe$, for a given doping level, temperature and cadmium fraction x, the reachable theoretical minority carrier lifetime depends on the type of doping [2] and determine the reachable diffusion dark current. HgCdTe extrinsic doping is a promising approach to reduce the diffusion dark current by reaching the Auger limit. In HgCdTe, this mechanism is mainly due to Auger 1 and 7 contributions [3], which are respectively preponderant in n and p doped materials [4].

The dark current in p-on-n HgCdTe photodiodes, with n-type absorber region, have been modeled by the empiric relationship “Rule 07” for SWIR to LWIR HgCdTe materials. The “Rule 07” describes the diffusion dark current density for a typical HgCdTe photodiode manufactured at Teledyne [5]. This relationship has be found to be consistent with an Auger 1 limitation of the minority carrier lifetime in MWIR to LWIR materials with an absorption layer characterized by a donor concentration in the 1.0×10^{15} cm^{-3} range [6]. The models used to predict the Auger 1 generation and recombination, the intrinsic carrier concentration and the corresponding diffusion dark current in n-type HgCdTe can therefore be considered to be well calibrated for MWIR to LWIR materials.

On the other hand, the achievable performance in extrinsically doped n-on-p photodiodes, with p-type absorber, is still to be determined. In HgCdTe, the Auger 1 recombination mechanism is more efficient than the Auger 7 mechanism [7]. Hence, a lower dark current can be theoretically reached in photodiodes with an extrinsically p-doped absorption layer

than with an extrinsically n-doped. The attainable gain is commonly modeled by the ratio between the Auger 1 and 7 recombination coefficients γ, which is greater than 1. However, the exact γ value is not yet known and, consequently, the reachable gain in dark current and/or operating temperature has yet to be determined. The development of MWIR n-on-p extrinsic HgCdTe photodiodes has been studied with dopant from group I such as Au and Cu and group V such as As [8]–[11]. These studies revealed challenges to reach the Auger 7 limitation unambiguously and the need to determine the doping level that minimizes the diffusion dark current. A clear estimation of the γ value from these studies seems difficult to conclude on since the doping and thickness of the absorption layer are not always reported. Moreover, the dark current is strongly dependent on the photodiode quality, such as the passivation [8], generating dispersion in the measured data. Similar issues are found with reported minority carrier lifetime, as the material quality and measurement precision may vary between publications [2]. Below "Rule 07" dark currents have been reported for MWIR n-on-p extrinsic photodiodes with As doping at a value around 1.5×10^{15} cm^{-3} [10]. The reported dark current densities at 200 K and 300 K are between 6 to 8 times below the "revisited Rule 07" from [6] respectively. However, a variation of the dark current and was reported for different photodiodes with the same doping [10]. This indicates the presence of extrinsic contributions to the dark current that can be present even in the device with the lowest dark current. In consequence, it is not guaranteed that the real Auger 7 limit has been reached. Moreover, the important 1/f noise associated to these photodiodes can be limiting for HOT applications. P-type extrinsic doping performances have also been demonstrated in the LWIR range where below "Rule 07" dark current densities have been reported [12], which confirms the interest of such photodiodes to reduce the dark current density even for devices with longer cutoff wavelengths. The doping level of the p-type layer was not reported for these photodiodes which is why no information on the Auger limit can be extracted from the dark currents.

The objectives of this study are to investigate the limit of extrinsic n-on-p HgCdTe photodiodes and to evaluate their potential for being used in HOT Focal Plane Arrays (FPAs). In view of these objectives, PhotoLuminescence Decay (PLD) mapping, Hall effect, dark current and dark current noise measurements have been performed on extrinsic p-type HgCdTe materials and photodiodes. Two doping levels of the p-type absorption layer have been studied in order to investigate its influence on the lifetime, the dark current density and to obtain an estimation of the value of γ in MWIR HgCdTe materials.

First, the studied samples and characterization tools are described. The following section presents minority carrier lifetimes, measured by PLD, and compared to models based on measured doping levels. Third, measured dark current densities are reported and compared with dark current densities calculated for Auger limited photodiodes and using measured minority carrier lifetimes. The perspective of using the present photodiode technology for HOT FPA applications is discussed in the following section, in view of results from dark current noise measurements that are compared with data reported from literature. The final section presents main conclusions that can be established from the present work and discuss the perspectives for using extrinsic n-on-p type HgCdTe photodiodes for HOT FPA applications.

2. MATERIALS AND METHODS

2.1 Materials

MWIR HgCdTe material from two different wafers, named A and B have been used in the present work. The HgCdTe layers were grown by liquid phase epitaxy on a [111]-CdZnTe substrate. The samples have been passivated and annealed to minimize the presence of metal vacancies in the sample that could contribute to the lifetime and dark current in the wafers.
For each wafer, two neighboring regions have been studied. A first region with photodiodes was used for electro-optical characterizations. The second region was a sample for Hall effect measurements with ohmic contacts situated at each corner. This sample was used for PLD and Hall effect measurements. Both the photodiode samples and the material characterization samples, used for PLD and Hall effect, are termed sample A or B in the following sections.

Photodiodes were formed by locally transforming the conductivity to n-type on a pitch of 15 µm. All the photodiodes have a planar-structure geometry. Studied components are hybridized on an interconnection circuit with indium bumps. The measured photodiodes are surrounded by neighboring photodiodes configured in two concentric rings. These neighboring photodiodes are referred to as the confinement ring. The role of these photodiodes is to confine the diffusion collection area around each measured photodiode. The resulting photodiode collecting area is approximately 15×15 µm².
The doping concentration is estimated by Hall effect measurements at liquid nitrogen temperature. Photodiodes cutoff wavelengths are determined at 80 K from Fourier Transform Infrared spectral response measurements on the photodiodes.

Results from these characterizations for each sample are presented in Table 1. The cadmium fractions are determined from the cutoff wavelength at 80 K using the expression proposed by Hansen [13]. Measured majority carrier concentrations p_0 at 77 K are used to model p_0 a higher temperature assuming a non-degenerated and uncompensated semiconductor material with an activation energy of 8.5 meV.

Table 1. Materials parameters of each sample studied in this work, p_0 is the majority carrier concentration in cm^{-3}.

Sample	**Estimated p_0 at 77 K (cm^{-3})**	**Cutoff wavelength at 80 K (µm)**	**Corresponding cadmium fraction using [13]**
A	6×10^{16}	5.12	0.299
B	2.5×10^{16}	5.30	0.294

2.2 Methods

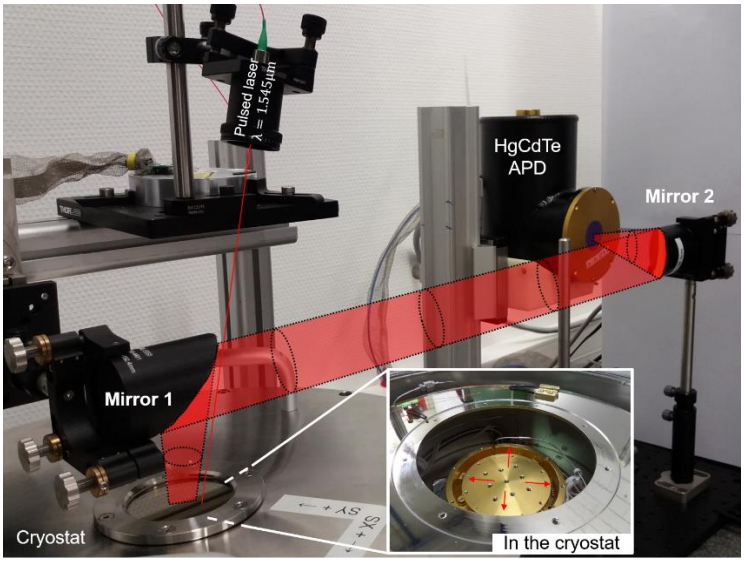

Figure 1. Photoluminescence decay mapping bench used to measure the minority carrier lifetime in this work.

The set-up for photoluminescence decay measurement is based on the one presented in [14]. Here, the samples are mounted on a temperature controlled 2-axes motorized stage that makes it possible to map the photoluminescence decay, and therefore the lifetime distribution, at the wafer scale, at variable temperature. This PLD mapping tool is presented in Figure 1. Excess carriers are photogenerated using a pulsed Erbium-doped fiber laser at a wavelength of 1.545 µm. The pulse frequency is 40 kHz and each pulse has a full width at half maximum of 1 ns. The pulsed signal is synchronized with the detection chain. The PLD signal is collected using two 3" off-axis parabolic mirrors. A germanium filter is placed before the detector to suppress the detection of scattered laser light that can saturate the detector. The temporal photoluminescence signal is recorded using an in-house HgCdTe Avalanche PhotoDiode (APD), that enables measuring the signal over large temporal and amplitude ranges, with an excess noise factor close to unity [15]. The APD is cooled down to 77 K, has a cutoff wavelength of 5.7 µm at 80 K and a reversed bias of -5.5 V is applied to obtain a gain around 50. The PLD signal is sampled at a frequency of 500 MHz and the signal is averaged 60000 times to improve the signal to noise ratio. The spatial resolution is estimated around 300 µm.

Equilibrium minority carrier lifetime is typically estimated from PLD curves by performing a mono-exponential fit in the low injection regime, which is reached at the end of the photoluminescence decay [16]. Note that the effective radiative lifetime may be increased due to photon recycling that depends on the sample preparation, such as the metallization of the sample surface. In the present work, no specific effort have been made to alter the photon recycling in the samples.

Current bias dependency (I-V) and current noise measurements are performed at variable temperature under dark conditions. Current noise measurements are performed at a fixed bias corresponding to the photodiodes maximum differential resistance that is determined from the measured I-V curves. During the measurements, the confinement ring photodiodes are kept at a fixed reverse bias value, close to the maximal differential resistance, in order to guarantee an effective collection of their dark current. At high dark current values, a de-biasing effect is observed due to the high current flowing through the confinement ring photodiodes. To keep the confinement effective on the central photodiode, the reverse bias of the confinement ring and the central photodiode are increased with temperature. A majority of the measured photodiodes have a typical behavior, without current leakage or noise current excess. Only the results measured on photodiodes with such typical behavior are studied and the measured median values of these photodiodes are presented in the following.

3. RESULTS AND DISCUSSION

3.1 Minority carrier lifetime measurement results

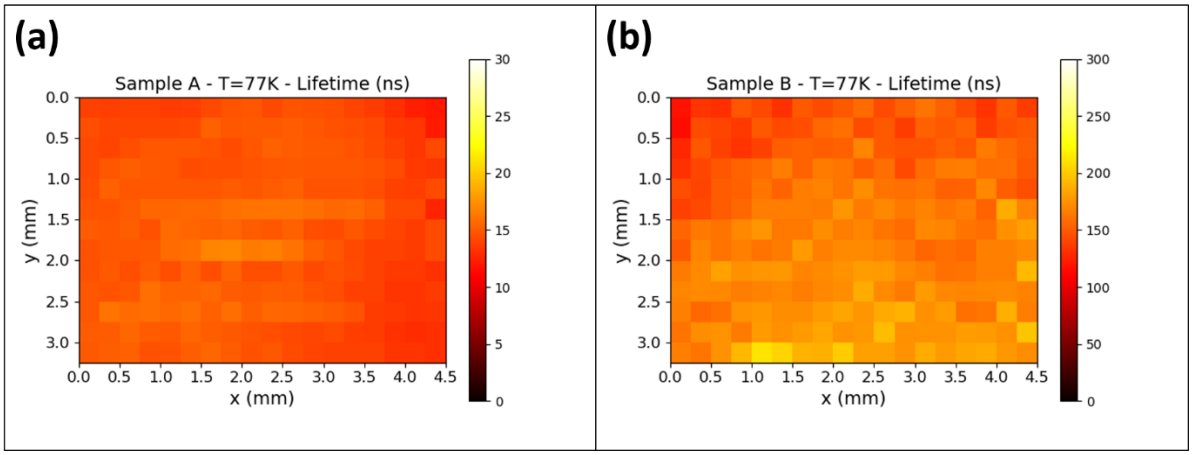

Figure 2. Minority carrier lifetime map at 77 K performed in the center of **a)** Sample A. **b)** Sample B. The measurement step is 250 µm.

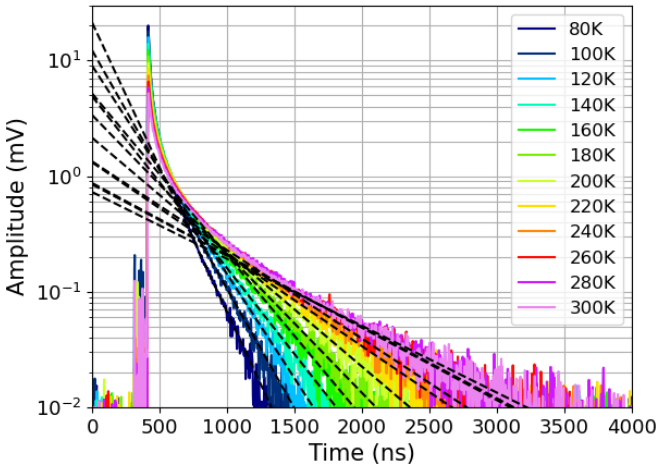

Figure 3. Photoluminescence decay curve measured at the center of sample B ($p_0 = 2.5 \times 10^{15}$ cm^{-3} at 77 K) for several temperatures and corresponding mono-exponential fit in low injection regime. For a better readability, only one out of two temperature are plotted.

At liquid nitrogen temperature, a complete mapping of both samples was performed with a step of 0.25 mm. Since our samples have electrical contacts at the edges, only a region of interest at the center of sample A and B of the measured lifetime maps are presented on Figure 2 (a) and (b).

Lifetime inhomogeneities on sample B are evidenced in Figure 2 (b) thanks to the 2D (x,y) PLD mapping capability. The lifetime variation can be due to doping inhomogeneities and/or spatial distribution of defects acting as Shockley–Read–Hall (SRH) recombination centers that degrade the lifetime locally. This issue could represent difficulties to develop a uniform FPA at this doping level. Figure 2 (a) shows that the spatial fluctuations on sample A are relatively lower. This difference can be correlated to the higher doping level in this sample. This observation could indicate that a lower spatial fluctuations in the performances of FPAs can be expected at higher doping levels. In the following, the average minority carrier lifetime estimated locally at the center of each sample are presented.

Figure 3 reports measured PLD curves at several temperatures for sample B. It can be seen that the PLD curves are characterized by a non-exponential behavior at the beginning of the decay. This behavior corresponds to the high carrier injection regime. The PLD curve ends with a mono-exponential decay associated with the low injection regime close to equilibrium. Even in this regime, the signal is more than one order of magnitude lower than the real time noise without averaging of the detector at an APD gain of 50. This shows the essential contribution from the in-house HgCdTe APD to obtain an accurate estimation of the minority carrier lifetime.

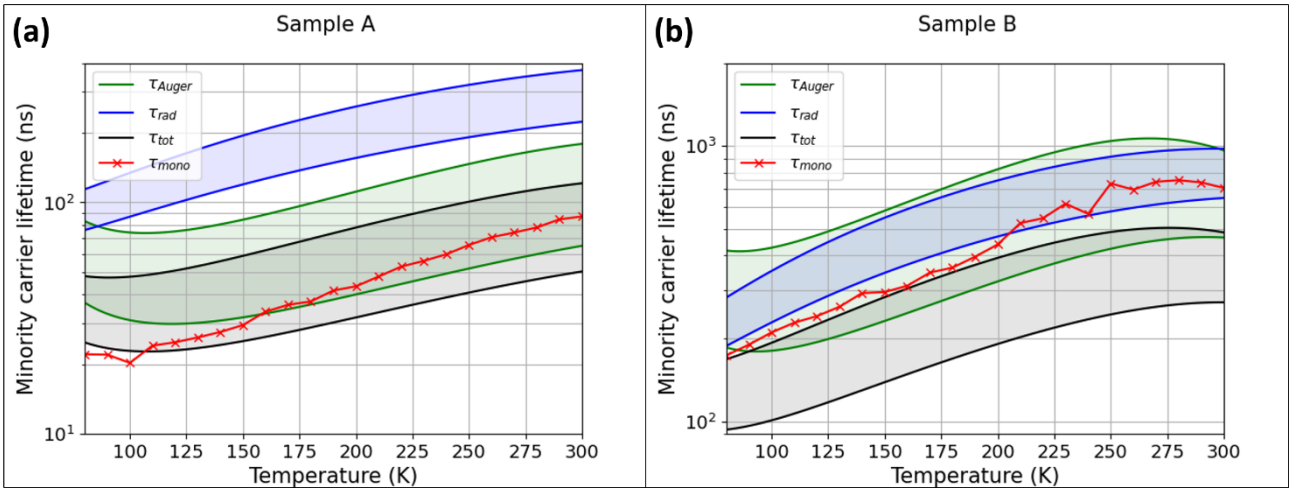

Figure 4. Measured (τ_{mono}) and modeled Auger and radiative lifetimes as a function of temperature for **a)** sample A and **b)** sample B. The different contributions to the lifetime are calculated assuming an uncertainty of measured doping by Hall effect of ± 20 %.

Figure 4 (a) and (b) report the lifetime τ_{mono} estimated from the measured PLD curves by performing a mono-exponential fit in the low injection regime, at variable temperature. The theoretical lifetime associated with radiative and Auger recombination mechanisms are calculated using models from [14]. To calculate the Auger lifetime, a γ value of 10 and an overlap integral of the interacting electron wave functions $|F_1F_2|$ of 0.2 are chosen [14]. The modeled Auger lifetime takes into account of both Auger 1 and 7 contributions. At the temperature range considered here, the modeled lifetime is limited by the Auger 7 contribution for both samples. Both photon recycling and SRH contributions are considered negligible. An uncertainty of the doping level measured by Hall effect of ± 20 % is assumed to calculate a range of expected lifetimes for each of the modeled recombination mechanisms.

Figure 4 (a) shows that, for sample A, the modeled total lifetime is higher than the measured values at low temperature and agrees with the measured lifetime at higher temperatures. For sample B, Figure 4 (b) shows that the measured lifetime is higher than the modeled values at all temperatures. Hence, the results for the two samples are not simultaneously consistent with the modeled lifetimes.

Two possible extreme explanations are proposed to explain this discrepancy:

- The first one is that the estimated doping level in sample A is correct and that the lifetime is dominated by intrinsic mechanisms. This implies that lifetime in this sample is limited by the Auger 7 mechanism, with a γ value slightly

lower than 10, to account for the lower lifetimes observed at low temperatures. However, to explain the sample B lifetime values, this would imply that the doping level in this sample is much lower than estimated and/or that the radiative lifetime is higher than predicted by the model. A higher radiative lifetime than predicted could possibly be due to photon recycling or a bad calibration of the model.

- The second possible explanation is that the estimated doping in sample B is correct. This means that $\gamma \geq 10$, to account for the longer measured lifetime in sample B and/or that the radiative lifetime is longer than expected in this sample. It do also imply that the lifetime in sample A is limited by an extrinsic SRH contribution and/or that it's doping level is higher than estimated.

A mix of the two extreme interpretations can also be used to explain the discrepancy. Unfortunately, current data do not make it possible to choose between the different explanations. The interpretation of these observations will be further discussed in section 3.2, where the measured lifetimes are compared to measured dark currents.

3.2 Dark current density measurement results

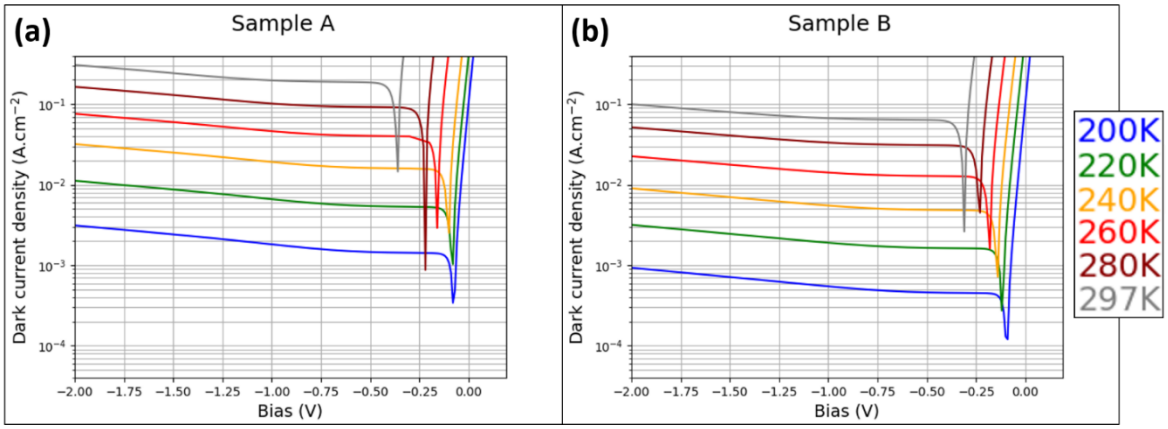

Figure 5. Measured dark current densities for both samples at several temperatures. The colormap refers to the temperature. **a)** Sample A. **b)** Sample B.

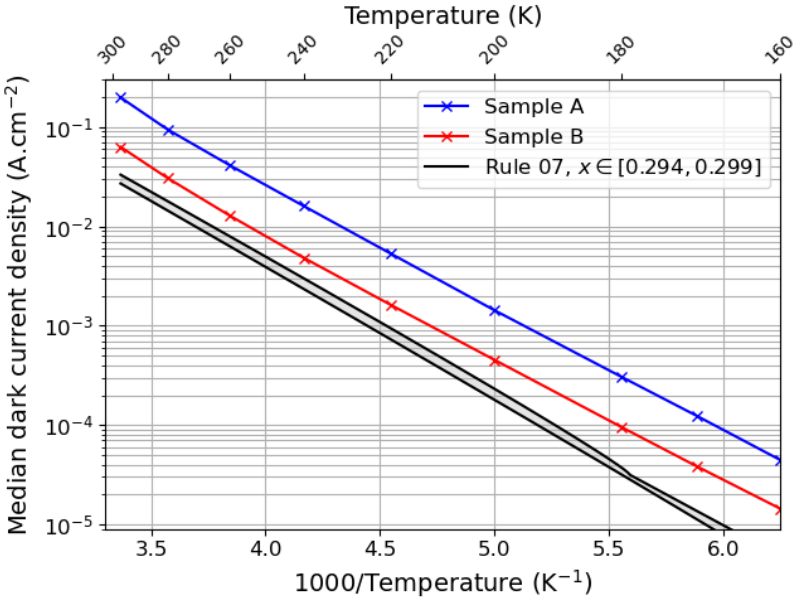

Figure 6. Measured median dark current densities for both samples and "Rule 07" as a function of reverse temperature.

Measured dark current densities as a function of bias at several temperatures are shown in Figure 5 for both samples. The variation of the measured median dark current densities from samples A and B are reported as a function of the reverse

temperature in Figure 6. The measured data are compared with values calculated using the "Rule 07", using coefficients from the "revisited Rule 07" [6]. The cutoff wavelength used within this model is calculated at each temperature using [13] with the cadmium fractions for each sample, reported Table 1. This figure shows that the dark current density in sample A is higher than in sample B. This is consistent with the lower doping and longer lifetime measured in sample B. It can also be seen that, at room temperature, the measured dark current density of sample B is between 1.6 and 1.9 times higher than Rule 07 and between 7.0 and 7.4 for sample A.
As mentioned in the introduction, "Rule 07" has been founded consistent with an Auger 1 limitation of photodiodes with a donor concentration in the 1.0×10^{15} cm^{-3} range in MWIR to LWIR materials [6]. However, in sample B which has a doping level one order of magnitude higher, comparable to "Rule 07" dark currents are measured. Since higher doping usually yields lower 1/f noise [17], a lower 1/f noise can be expected with this technology compared to "Rule 07" p-on-n photodiode despite the slightly higher dark currents. This aspect will be further discussed in section 3.2, where measured dark current noise is presented. Furthermore, these results indicates that an even lower dark current could be obtained in a photodiode with lower p-doping, if the observed reduction in dark current as a function of doping is confirmed.

In order to investigate the origin of the limitations to the dark current in our photodiodes, the measured dark currents are compared with the expected Auger limited dark current and the dark current calculated from lifetime measured by PLD. In a diffusion-limited photodiode in reverse bias, which is the case at high operating temperature, the diffusion dark current density $J_{\text{dark diffusion}}$ in A.cm^{-2} is given by (supposing a p-type absorber) [1]:

$$J_{\text{dark diffusion}} = \frac{ezn_i^2}{p_0\tau} \tag{1}$$

where e is the elementary charge in C, z is the thickness of the absorption layer in cm, n_i is the intrinsic concentration in cm^{-3}, p_0 is the majority carrier concentration in the absorption layer (which is p-doped for a n-on-p photodiode and would be noted n_0 for a p-on-n photodiode) in cm^{-3} and τ is the minority carrier lifetime at equilibrium in the absorption layer in s. It has to be noted that equation 1 is valid only if $z < L_D$ where L_D is the diffusion length of the minority carriers in the absorption region. The measured dark current densities are compared to modelled diffusion dark current densities using equation 1 in Figure 7. The intrinsic carrier concentration n_i is computed using [18].

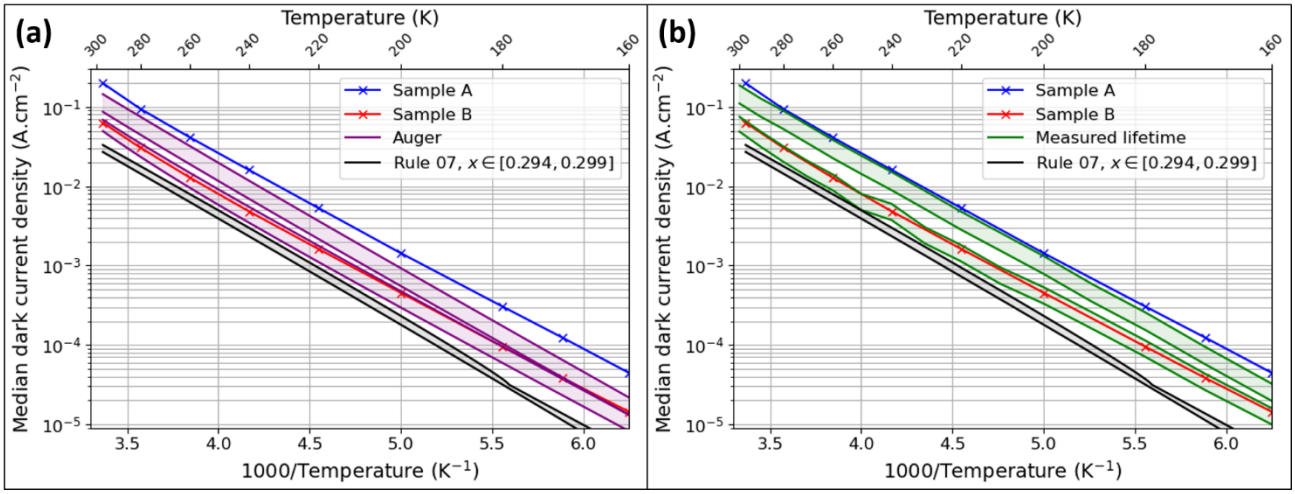

Figure 7. Median measured and modeled diffusion dark current densities for both samples and "Rule 07" as a function of reverse temperature and modeled diffusion dark current density using equation 1 as a function of reverse temperature. Errorbars represent an uncertainty of measured doping of ± 20 %. **a)** Diffusion dark current modelled for an Auger-limited photodiode. The higher the doping level is, the higher the dark current density is. **b)** Diffusion dark current modelled from measured lifetime presented in Figure 4. The highest/lowest dark current modelled are associated to sample A/B respectively.

In Figure 7 (a), the dark current has been modelled supposing an Auger limited lifetime with $\gamma = 10$. The physical parameters used to model the lifetime are presented in section 3.1. For sample B, measured dark current densities are consistent with the upper limit given by the modeled Auger limited dark current. However, measured dark current on sample A is higher than the modeled dark current density.

Figure 7 (b) shows a similar trend for the dark current densities calculated using the measured lifetimes. In presence of an important contribution of radiative recombination to the measured lifetime, the direct use of the measured lifetime could lead to an overestimation of the photodiode dark current, to which the radiative contribution on the dark current is expected to be negligible in a well confined photodiode [2].

These observations are not compatible with the first explanation deducted from the measured lifetime in section 3.1. In this explanation, the doping level in sample A is assumed to be correct and the lifetime is limited by Auger recombination, with a γ value slightly lower than 10. Figure 7 (a) and (b) show that measured dark current densities are higher than the modeled values for sample A. This hypothesis is not compatible with the difference between the measured and calculated dark current from lifetime measured by PLD in Figure 7 (b). This difference can only be explained supposing a reduced doping in sample A.

A better agreement with the measured dark currents in samples A and B is found for the second explanation deducted from the measured lifetime. In this explanation, the doping level in sample B is assumed to be correct. This assumption implies a value of $\gamma \geq 10$ and/or longer radiative lifetime for this sample. It do also imply that the lifetime in sample A is limited by an extrinsic SRH contribution and/or that its doping level is higher than estimated. However, if the doping level of sample A is higher, then predicted dark current from measured lifetime would be even lower. This indicates that the lifetime in sample A is most likely SRH limited and associated with a doping which is slightly lower than estimated. Concerning sample B, the consistency of the measured lifetimes with the measured dark current indicate, within this picture, that the radiative contribution to the measured lifetime is lower than the one predicted by the model. This could be explained by a bad calibration of the radiative lifetime model and/or the presence of photon recycling in sample B.

Another explanation, where the doping level of sample B is lower than estimated, is also compatible with measured lifetime. In this case, the dark current calculated with the measured lifetime would be consistent with measured dark current through a reduced radiative contribution to the measured lifetime. In addition, the Auger lifetime needs to be compensated by a reduced γ value below 10 to ensure consistency between modeled Auger dark current and measured dark current. As this would imply a larger error than 20 % on the doping level, we consider this explanation is less likely to be correct than the second explanation.

In conclusion of this section, the combined analysis of Hall effect, PLD and measured dark current show that the results are most consistent with an γ value around 10, a lower than expected radiative recombination and additional SRH contribution at a higher doping level. This last conclusion can, for example, be explained by the formation of complexes of dopants in the epitaxial layer which act as SRH centers that degrades the total lifetime. Similar measurements need to be performed on samples with intermediate and higher doping levels to confirm this hypothesis.

3.3 Dark current noise density measurements results

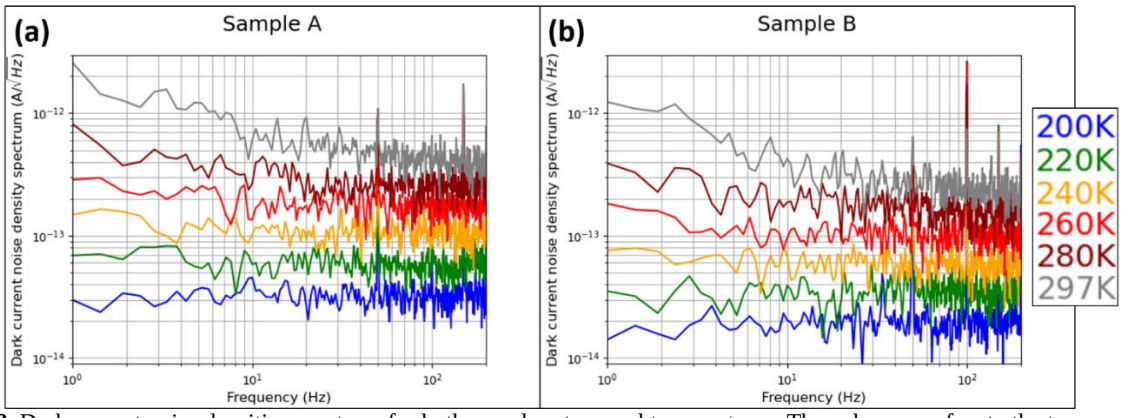

Figure 8. Dark current noise densities spectrum for both samples at several temperatures. The colormap refers to the temperature. **a)** Sample A. **b)** Sample B.

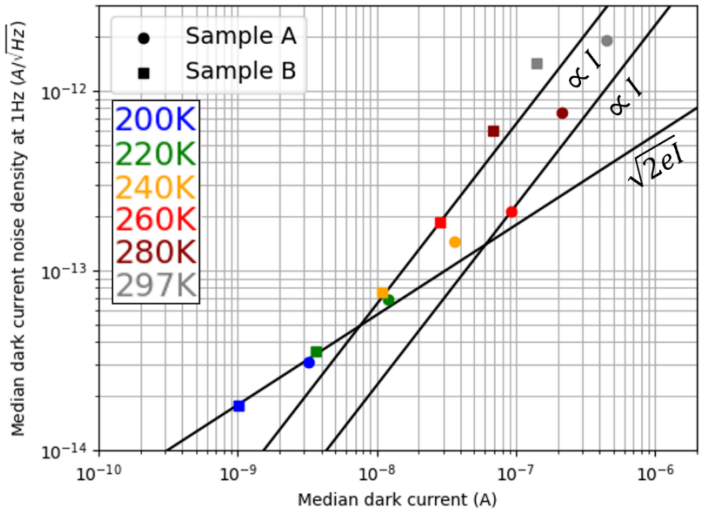

Figure 9. Median dark current densities at 1 Hz as a function of median dark current at several temperatures. The solid black lines correspond to the shot noise given by equation 2 and to the linear relashionship given by equation 3 using the median Tobin coefficient at 1 Hz α at 260 K (see text for discussion).

Figure 8 presents typical dark current noise spectra measured at variable temperature for photodiodes in samples A and B. The dark current noise spectra plotted in Figure 8 (a) and (b) are associated with photodiodes presented in Figure 5 (a) and (b) respectively. It can be seen that a close to white noise, corresponding to the expected shot noise of the dark current, is observed at temperatures less than approximately 220 K. 1/f noise is observed at higher temperatures. The onset of low frequency noise at such high temperature is of great interest for high operating temperature applications.

In Figure 9, median dark current noise density at 1 Hz is plotted as a function of the median dark current for both samples. The solid black line labelled $\sqrt{2eI}$ corresponds to the classical shot noise $i_{n_{\text{shot noise}}}$ in A.Hz$^{-1/2}$ given by equation 2:

$$i_{n_{\text{shot noise}}} = \sqrt{2eI} \qquad (2)$$

where e is the elementary charge in C, I is the dark current delivered by the photodiode in A. It can be seen that both samples A and B are shot noise limited up to 220 K.

To quantify the photodiodes performances, it is convenient to model the current noise density i_n in A.Hz$^{-1/2}$ with a relationship proposed by Tobin *et al.* [19] :

$$i_n = \frac{\alpha I}{\sqrt{f}} \qquad (3)$$

where f is the frequency in Hz, α is a dimensionless coefficient named Tobin coefficient and I is the current delivered by the photodiode in A. Median Tobin coefficients at 1 Hz α have been computed using equation 3 with $f = 1$ Hz for temperatures presented in Figure 9. The corresponding linear trend of the dark current density i_n given by equation 3 is plotted in Figure 9 using the median Tobin coefficient α at 260 K. It can be seen that the measured current noise density at 1 Hz is not proportionnal to the dark current at high temperature for both samples and increases faster than the linear relationship given by equation 3. Computed values of Tobin coefficients α at 260 K and higher temperatures are summarized in Table 2. The non linear variation of the current noise density at 1 Hz as a function of the dark current shows on a limit to use the Tobin coefficient estimated at room temperature to predict the stability of the detector at lower temperatures. In the present case, the faster decrease of 1/f noise at lower temperatures suggests a higher stability of the dark current at lower temperature than what can be extrapolated from the room temperature value.

Figure 9 shows that a given dark current, the dark noise density at 1 Hz is higher for sample B than for sample A. This result is consistent with the doping dependence of the 1/f noise reported in intrinsic n-on-p HgCdTe photodiodes [17].

However, at a given temperature, the median dark current noise density at 1 Hz and median dark current of sample A are higher than for sample B showing that an improved performance is observed for this sample although the improvement is not proportional to the reduction in dark current. This result shows on a possible limitation in performances at lower doping levels than the once studied here.

For an ideal detector (with an ideal quantum efficiency), the photon current density associated to a numerical aperture of F/4 and a cutoff wavelength of 4.8 µm at 165 K is 2×10^{-5} A.cm^{-2}. On sample B, Figure 6 from section 3.2 shows that this current is observed around 165 K. Thus, the Background Limited Performance (BLIP) temperature of sample B at F/4 is 165 K. At this temperature, the dark current noise level is below the instrumental resolution. However, as the photodiodes are shot noise limited below 220 K and characterized by a low 1/f noise at higher temperatures, high stability and high performances of these photodiodes can be expected at the 165 K BLIP temperature.

Table 2. Median Tobin coefficients at 1 Hz α measured at 260 K, 280 K and 297 K for both samples.

	Sample A	**Sample B**
260 K	2.3×10^{-6}	6.5×10^{-6}
280 K	3.6×10^{-6}	8.7×10^{-6}
297 K	4.3×10^{-6}	1.0×10^{-5}

3.4 Comparison with state of the art HgCdTe MWIR photodiodes

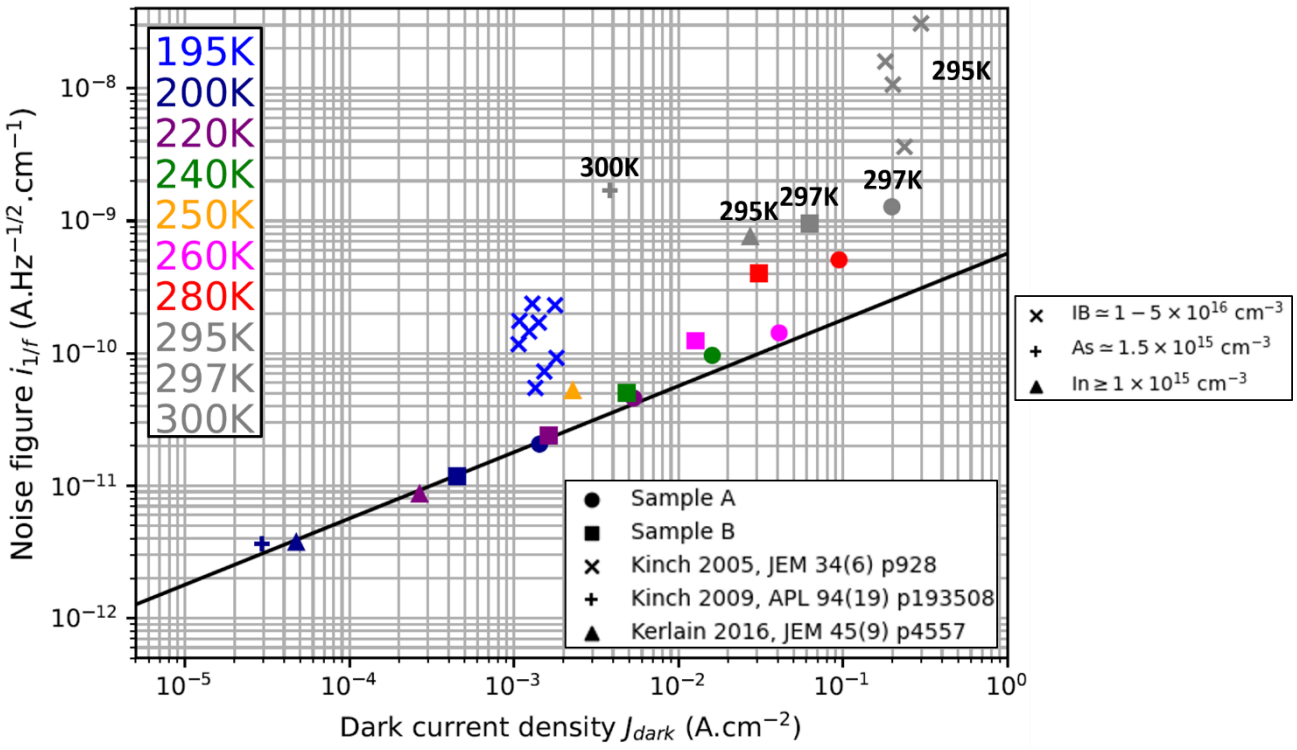

Figure 10. Normalized to the square root of the area dark current noise density at 1 Hz noise figure $i_{1/f}$ as a function of dark current density J_{dark} at several temperatures for photodiodes presented in this work and data reported in literature. Literature data correspond to n-on-p extrinsic photodiodes manufactured at DRS from [10], [20] and p-on-n extrinsic photodiodes developed at the DEFIR laboratory [21]. The colormap refers to the temperature. At the highest temperatures, the same colormap is used for a better readability. The solid black line corresponds to the shot noise calculated using equation 2 with the dark current density J_{dark} in A.cm^{-2}.

To compare our photodiodes performances with reported data from literature, dark current noise densities at 1 Hz are normalized to the square root of the collecting area of the photodiodes. This noise figure, presented in [20], is labelled $i_{1/f}$. The $i_{1/f}$ noise figure is plotted as a function of dark current density J_{dark} in Figure 10. The measured noise figures are

compared to values reported values for extrinsically p-doped photodiodes reported by DRS [10], [20] and for extrinsically n-doped photodiodes developed at the DEFIR laboratory (joint laboratory of Lynred and CEA-Leti) by Kerlain [21]. Photodiodes reported by Kerlain were made in blue MWIR material with a shorter cutoff wavelength for IR detection up to 4.2 µm. The type of dopant and associated doping level of devices from literature are represented in Figure 10, where IB refers to an impurity from the IB group.

It can be seen that, around 300 K, $i_{1/f}$ reported by Kinch 2005 [20] are between 3 to 24 times higher than sample A approximately, with a similar J_{dark}. At 200 K, both photodiodes from samples A and B are shot noise limited while data reported in Kinch 2005 [20] exhibit a $i_{1/f}$ between approximately 3 to 12 times higher than the shot noise value at 195 K. Since photodiodes reported by Kinch 2005 [20] have a doping level similar to photodiodes from samples A and B, this result highlights the noise performances of the present devices. It could be explained by differences associated to the photodiode process steps, such as the passivation and junction formation.

At 200 K, the photodiodes in samples A and B have shot noise behavior similar to the one reported in Kinch 2009 [10] although samples A and B have a higher J_{dark}. The difference in dark current can be attributed to their difference in doping level. However, at temperatures around 300 K our photodiodes have higher J_{dark} but lower $i_{1/f}$, showing on a more stable performance of the present devices at high operating temperature. As before, it can also be explained by differences in the photodiode process steps.

The comparison with p-on-n photodiodes from Kerlain 2016 [21] shows that at 200 K and 220 K, both photodiodes types display shot noise limitation. The current of the present n-on-p photodiodes is higher, which can be attributed to the difference in cutoff wavelength and doping levels. Measured J_{dark} for sample B at 280 K is similar to J_{dark} reported in Kerlain 2016 [21] at 295 K but its $i_{1/f}$ is lower by a factor around 2.

These comparisons and the extrapolation of the data reported in Figure 10 show that, at a given J_{dark}, the photodiodes from samples A and B have lower $i_{1/f}$ than reported values from literature. Thus, the n-on-p extrinsic photodiode technology presented in this work is promising for HOT FPA applications.

4. CONCLUSION

Extrinsically doped n-on-p MWIR HgCdTe photodiodes from two wafers with two doping level of the absorption layer have been studied using PLD, Hall effect and dark current and dark current noise measurements.
The correlation of the dark current measurements, models of the lifetime and dark current is compatible with a γ value around 10, a lower than expected radiative recombination and an additional SRH contribution at higher doping level.

Measured dark current noise and dark current have shown a shot noise limited behavior up to around 220 K for both samples. At high temperature, the dark current noise increases faster than the dark current in both samples. The lowest measured median Tobin coefficient α at 1 Hz is 2.3×10^{-6} at 260 K for sample A with a doping level around 6×10^{16} cm^{-3} at 77 K. At room temperature, an α value of 4.3×10^{-6} is measured for this sample. This level of relative low frequency noise is, to the best of our knowledge, the lowest value that has been reported for diffusion limited HgCdTe photodiodes.

A BLIP temperature of 165 K at F/4 has been estimated for sample B with a doping level around 2.5×10^{16} cm^{-3} at 77 K. The low values of 1/f noise at higher operating temperature indicate that the detector noise is expected to be shot noise limited at this temperature, with a low influence of the low frequency noise on the image quality even on very long time scales. Further, the low 1/f current noise densities opens a perspective to reduce the doping level in order to reduce the dark current. At $\gamma = 10$, and a doping level of 1×10^{15} cm^{-3} , the dark current is expected to be reduced by a factor 25 in comparison with sample B. This will increase the BLIP temperature of an FPA at F/4 to 190 K. Such high operating temperature would be a breakthrough for SWAPc applications, at the condition that a low 1/f noise is conserved at lower doping and that the doping level is homogeneous over the surface of the FPA.

REFERENCES

[1] Kinch, M. A., [Fundamentals of Infrared Detector Materials], Bellingham, WA: SPIE Press, (2007).

[2] Kinch, M. A., Aqariden, F., Chandra, D., Liao, P.-K., Schaake, H. F., and Shih, H. D., "Minority carrier lifetime in p-HgCdTe," J. Electron. Mater. 34(6), 880-884 (2005).

[3] Rogalski, A., [Infrared Detectors], 2nd ed., Boca Raton: Taylor & Francis, (2011).

[4] Casselman, T. N., and Petersen, P. E., "A comparison of the dominant Auger transitions in p-type (Hg,Cd)Te," Solid State Commun., 33(6), 615-619 (1980).

[5] Tennant, W. E., Lee, D., Zandian, M., Piquette, E., and Carmody, M., "MBE HgCdTe Technology: A Very General Solution to IR Detection, Described by "Rule 07", a Very Convenient Heuristic," J. Electron. Mater. 37(9), 1406-1410 (2008).

[6] Tennant, W. E., ""Rule 07" Revisited: Still a Good Heuristic Predictor of p/n HgCdTe Photodiode Performance?," J. Electron. Mater. 39(7), 1030-1035 (2010).

[7] Krishnamurthy, S., and Casselman, T. N., "A detailed calculation of the auger lifetime in p-type HgCdTe," J. Electron. Mater. 29(6), 828-831 (2000).

[8] Schirmacher, W., Wollrab, R., Lutz, H., Schallenberg, T., Wendler, J., and Ziegler, J., "Processing of LPE-Grown HgCdTe for MWIR Devices Designed for High Operating Temperatures," J. Electron. Mater. 43(8), 2778-2782 (2014).

[9] Kinch, M. A., Schaake, H. F., Strong, R. L., Liao, P. K., Ohlson, M. J., Jacques, J., Wan, C.-F., Chandra, D., Burford, R. D., and Schaake, C. A., "High operating temperature MWIR detectors", Proc. SPIE. 7660, 76602V (2010).

[10] Kinch, M. A., Wan, C.-F., Schaake, H., and Chandra, D., "Universal 1/f noise model for reverse biased diodes," Appl. Phys. Lett., 94(19), 193508 (2009).

[11] Knowles, P., Hipwood, L., Shorrocks, N., Baker, I. M., Pillans, L., Abbott, P., Ash, R. M., and Harji., J., "Status of IR detectors for high operating temperature produced by MOVPE growth of MCT on GaAs substrates," Proc. SPIE. 8541, 854108 (2012).

[12] Haiml, M., Eich, D., Fick, W., Figgemeier, H., Hanna, S., Mahlein, M., Schirmacher, W., and Thöt, R., "Low dark current LWIR HgCdTe focal plane arrays at AIM," Proc. SPIE. 9881, 988116 (2016).

[13] Hansen, G. L., Schmit, J. L., and Casselman, T. N., "Energy gap versus alloy composition and temperature in $Hg_{1-x}Cd_xTe$," J. Appl. Phys. 53(10), 7099-7101 (1982).

[14] Delacourt, B., Ballet, P., Boulard, F., Ferron, A., Bonnefond, L., Pellerin, T., Kerlain, A., Destefanis, V. and Rothman, J., "Temperature and Injection Dependence of Photoluminescence Decay in Midwave Infrared HgCdTe," J. Electron. Mater. 46(12), 6817-6828 (2017).

[15] Rothman, J., de Borniol, E., Abergel, J., Lasfargues, G., Delacourt, B., Dumas, A., Gibert, F., Boulade, O., and Lefoule, X., "HgCdTe APDs for low-photon number IR detection," Proc. SPIE. 10111, 1011119 (2017).

[16] Jenkins, G. D., Morath, C. P., and Cowan, V. M., "In-situ minority carrier recombination lifetime measurements at radiation sources for rad-hard IR detector materials," Proc. SPIE. 9226, 92260S (2014).

[17] Hassis W., Gravrand, O., Rothman, J., and Benahmed, S., "Low-Frequency Noise Characteristics of HgCdTe Infrared Photodiodes Operating at High Temperatures," J. Electron. Mater. 42(11), 3288-3296 (2013).

[18] Hansen, G. L., and Schmit, J. L., "Calculation of intrinsic carrier concentration in $Hg_{1-x}Cd_xTe$," J. Appl. Phys. 54(3), 1639-1983 (1983).

[19] Tobin, S. P., Iwasa, S., and Tredwell, T. J., "1/f Noise in (Hg, Cd)Te photodiodes," IEEE Trans. Electron Devices 27(1), 43-48 (1980).

[20] Kinch, M. A., Wan, C.-F., and Beck, J. D., "1/f noise in HgCdTe photodiodes," J. Electron. Mater. 34(6), 928-932 (2005).

[21] Kerlain, A., Brunner, A., Sam-Giao, D., Pére-Laperne, N., Rubaldo, L., Destefanis, V., Rochette, F., and Cervera, C., "Mid-Wave HgCdTe FPA Based on P on N Technology: HOT Recent Developments. NETD: Dark Current and 1/f Noise Considerations," J. Electron. Mater. 45(9), 4557-4562 (2016).